Computational Study of Water Adsorption on Halloysite Nanotube in Different pH Environments

Riccardo Rozza[a], Francesco Ferrante[b,*]

[a] *Dipartimento di Fisica e Astronomia "E. Majorana" - Università degli Studi di Catania, Via S. Sofia 64, 95123 Catania, Italy*
[b] *Dipartimento di Fisica e Chimica "E. Segrè" - Università degli Studi di Palermo, Viale delle Scienze Ed. 17, 90128 Palermo, Italy*

Abstract

The comprehension of structural and energetic features of halloysite nanotube (HNT) in different chemical environments plays a crucial role in developing new HNT based materials. So far these aspects were investigated by means of laboratory techniques that hardly are able to provide hints at atomistic level of detail. Our investigation aims to obtain such accurate informations through density functional theory calculations on HNT models, in order to figure out the most stable forms of HNT under different pH conditions. It turns out that, at low pH, the preferred protonation sites are located in the inner aluminic surface while in alkaline medium the silicic layer can show delocalized negative charges due to the formation of silanol groups. The adsorption of water molecules (WMs) on the HNT inner and outer surfaces in acidic and alkaline environments was investigated as well, so characterizing the hydrogen bonds which determine the adsorption geometry. Further, calculations allowed to verify how the modification of one layer affects the energetics of water adsorption on the other one.

Keywords: Halloysite, Density Functional Theory, Water, Hydrogen Bonds

*Corresponding author
Email addresses: riccardo.rozza@phd.unict.it (Riccardo Rozza), francesco.ferrante@unipa.it (Francesco Ferrante)

1. Introduction

Halloysite is a clay material arranged in a nano-scroll shape with stoichiometric formula $Al_2Si_2O_5(OH)_4 \cdot nH_2O$, (n = 0, 2). It is made up of an external layer of silicon oxide and an internal one of aluminum hydroxide. The distance between the branches of the spiral can be 7 or 10 Å, when none or two interarms water molecules are structurally involved, respectively. The inner cavity size is generally comprised between 15 and 100 nm, while the nanotube walls thickness is determined by the number of windings around the nanotube axis and it is usually between 50 and 150 nm. The HNT morphology depends on the extraction site (Joussein et al., 2005; Pasbakhsh et al., 2013) and, compared to other clay materials, e.g. kaolinite, HNT nanotubes show a much higher surface area (Yuan et al., 2015). The easy availability, the cheap production cost and the bio-friendly behaviour (Vergaro et al., 2010; Fakhrullina et al., 2015; Fakhrullin & Lvov, 2016; Bertolino et al., 2017) make HNT one of the most exploited aluminosilicate. The applications are manifold: HNT can be used in pollutants removal (Núñez-Delgado et al., 2015; Massaro et al., 2016; Anastopoulos et al., 2018), controlled release and self-healing materials (Lvov et al., 2008; Shchukin et al., 2008; Fakhrullin et al., 2014; Rozza et al., 2019), catalysis (Wang et al., 2015; Massaro et al., 2017; Lazzara et al., 2018) and photocatalysis (Papoulis, 2019), drug delivery (Lvov et al., 2016b; Lisuzzo et al., 2019), and polymer and material science (Guo et al., 2008; Lin et al., 2011; Lvov et al., 2016a; Gaaz et al., 2017). Besides, the HNT inner lumen dimension can actually be tuned in order to enhance its loading capacity: for example, in acidic solution the inner lumen is enlarged and the HNT loading increases up to three times its normal value (White et al., 2012; Zhang et al., 2012; Abdullayev et al., 2012). The list of the halloysite-based materials applications is extremely long and all the aforementioned features contribute to enlarging this range more and more every day.

Despite the interest of both scientific and industrial community, something is still unknown about HNT structure and behaviour. As an example, the reason

that leads to the spiral shape is still under debate, even if some steps were done in revealing this issue (Prishchenko et al., 2018). In particular, in a previous work (Ferrante et al., 2015) we hypotesized, on the basis of a computational investigation on HNT nanotube models, that the winding of a kaolinite sheet generating a spiral structure in presence of water (i.e. halloysite-10Å) could be driven by the formation of a dynamic H-bonds linkage between the arms of the spiral, mediated by WMs. The very same nature of the geometric spiral gives rise to a lattice that is not strictly periodic in the winding direction, which in turn causes a disordered H-bonds network. As a result, the water molecules in the interarms region can adapt their orientation to realize the best interactions between the silicic and aluminic layers, an event that could not occur in a periodic superposition of unfolded kaolinite sheets (which would result in a hypothetical kaolinite-10Å).

A primary importance process involved in HNT applications is the adsorption of molecules onto the HNT surfaces, which is directly influenced by the chemical environment. Unfortunately the usual experimental techniques do not provide atomistic details about the consequence of a structural modification on a single HNT surface. The only deducible things are the changes taking place on the whole HNT system and not on single chemical sites (Bretti et al., 2016). Computational chemistry is a big hand of help in providing useful hints about the latter point. In smart material design, to know in advance the behaviour of a material after a chemical modification is an added value: it could allow to discriminate whether or not is worthwhile to invest resources on a particular project. Joint computational and experimental works could be the key in developing new materials in the most efficient way. As an example, some attempts in creating new self-healing material on unmodified HNT were done in an our previous study (Rozza et al., 2019), where composites between HNT and two corrosion inhibitors, quinaldic acid and salicylaldoxime, were proposed.

Most exploited HNT-composites synthesis are conducted in water at different pH values. In this work the structural and electronic properties of charged and uncharged HNT surfaces, as well as the characteristics of water adsorption on

pristine and modified HNT, were evaluated. The acquired information allowed us to establish a scale of the most stable HNT forms when different superficial charges are present on its surface.

2. Computational Details and Models

The HNT structures as well as the WM adsorption on HNT were investigated by means of Density Functional Theory with the M06-L exchange-correlation functional (Zhao & Truhlar, 2006), which was preferred to the M06-2X, or other hybrid functionals based on meta-GGA, because it allows to use the resolution of identity technique (RIDFT) for the evaluation of the integrals needed. The RIDFT approach scales almost quadratically with respect to the number of atomic basis functions and helps to reduce the computational cost when DFT is applied to large size systems (Eichkorn et al., 1995, 1997). The valence double-ζ plus polarization basis set (VZP) created by Ahlrichs and co-workers (Schäfer et al., 1992) was employed, that has the following contraction schemes: H (4s1p)/[2s1p]; O(7s4p1d)/[3s2p1d]; Al, Si(10s7p1d)/[4s3p1d]. The auxiliary functions corresponding to the VZP basis set were used for RI approximation. The basis set superposition error (BSSE) was estimated for every investigated system through the counterpoise procedure (Boys & Bernardi, 1970). All the calculations reported in the present work were performed with the Gaussian 09 software (Frisch et al., 2009).

The HNT structures and WMs adsorption investigation have been made through a cluster approach by using a portion (see Figure 1) taylored from a nanotube model obtained in a previous study via DFTB calculations (Ferrante et al., 2015) and described in details in (Ferrante et al., 2017). The dangling bonds were saturated with hydrogen atoms, while the aluminum and silicon ones placed at the edge were kept fixed in their positions in order to reproduce the HNT curvature. This model was used both for chemical modifications and WM adsorption. The model is large enough to ensure that edge effects will not interfere with any process (Ferrante et al., 2017; Rozza et al., 2019). The ge-

ometry optimization of the WM/HNT systems started with the water molecule placed at the center of the surface, so maximizing the number of interactions of the WMs with oxygen and hydrogen atoms. In the case of charged surfaces, the WM is placed near the modification.

[Figure 1 about here.]

The WMs interact via H-bond with the HNT surfaces, and the possible presence of a superficial charge adds charge-dipole interactions. The following notation (mostly used in figures) will be employed to describe hydrogen bonds: i) the distances (r) will be expressed in Ångströms and the angles (a) in degree, according to the scheme XHY(r,a); ii) H-bond as donor or as acceptor are represented as XH-Y or X-HY, respectively; iii) the left side of the notation is referred to atomic centers belonging to a WM, the right side to atoms of the surface. The donor-acceptor behaviour between water molecules themselves will be explicated when needed. The interactions described in this work have $r < 3.0$ Å and $140^\circ < a < 180^\circ$; all other interactions will be considered as secondary and will be discussed only if needed.

In order to avoid redundancies, a special notation is settled for the differently charged HNT systems. When a single proton is attached to a layer, the system will take the label HNT(AlO-H) or HNT(SiO-H) for the silicic or aluminic layer protonation, respectively. The double protonation can occur on different layers, HNT(AlO-H/SiO-H), or on the same layer, HNT(AlO-H/AlO-H) and HNT(SiO-H/SiO-H). In order to identify the relative position of two protons, the system will be labelled in an organic chemistry-like way, referring to the oxygen atoms hexagon on top of both surfaces. Thus the double protonated systems will be named HNT(AlO-H/AlO-H,x), where x is -ortho (o), meta (m) or para (p); the same notation is adopted for the silicic layer. A negative charge on aluminic layer is realized through a single, double or triple proton removal; the short system name will be HNT(AlO^{n-}), where n is the superficial charge. The creation of a negative charge on the silicic layer is not so intuitive and its genesis pass through a silanol formation, so its label is HNT(Si-OH). A dipole through the

spiral arms can occur when the Al layer carries a negative charge and the Si one is positively charged or vice versa. In the former case we will refer to the system with the short name HNT(AlO^-/SiO-H), in the latter with HNT(AlO-H/Si-OH). Finally, the system with a negative charge of both HNT surfaces is named HNT(AlO^-/Si-OH). A brief summary is presented for the sake of clarity:

HNT - uncharged Halloysite nanotube

HNT(AlO-H) - H^+ on Al layer

HNT(SiO-H) - H^+ on Si layer

HNT(AlO-H/AlO-H,x) - two H^+ on Al layer in (x = o, m, p) position

HNT(SiO-H/SiO-H,x) - two H^+ on Si layer in (x = o, m, p) position

HNT(AlO^{n-}) - n-times deprotonated Al layer

HNT(Si-OH) - negative charged Si layer

HNT(AlO^-/SiO-H) - first type of dipole on HNT

HNT(AlO-H/Si-OH) - second type of dipole on HNT

HNT(AlO-H/SiO-H) - both Al and Si layers positively charged

HNT(AlO^-/Si-OH) - both Al and Si layers negatively charged

The notation for the WM adsorption occurring on these systems is W-(HNT system) or W_2-(HNT system), depending on the number of water molecules involved. In order to shorten the notation, the abbreviation HNT will be omitted in naming systems with WMs, e.g. the adsorption of a WM on the silicic surface with one superficial charge will be labelled simply W-SiO-H.

3. Results and Discussion

3.1. HNT structures

The first part of the investigation is dedicated to the energetic of the HNT structural modifications due to a different pH environment. The energy vs su-

perficial charge trend is graphically reported in Figure 2, whose detailed description is going to be provided. Incidentally, the scheme shows only the energies of the charged halloysite models with respect to the pristine form; in order to obtain the energetic of the processes that originate the charged systems, it must be recalled that the formation of positively charged species involves the dissociation of H_3O^+, which, according to the calculation method used in the present investigation, requires 742.5 kJ mol^{-1} of energy; on the other hand, the creation of the negatively charged species occurs together with the formation of water from OH^- and the extracted H^+, which releases 1826.1 kJ mol^{-1} of energy.

For the discussion that follows, it is worthwhile to report some information about the model representing the uncharged HNT, to be used as reference. In the inner layer of this system, the Al-O distances goes from 1.89 to 1.93 Å and the O-H bonds are 0.96 Å long. The hydrogen atoms of the hydroxyl groups in para between each other point toward the same direction. On the silicic layer the Si-O distances are in the narrow range 1.65-1.66 Å. The molecular electrostatic potential calculated for the uncharged HNT (Fig. 1b) shows negative values on the silicic surface and positive ones on the gibbsitic layer, in agreement with experimental evidences.

It is worthwhile to remember here that at given pH values the leaching of HNT can occur, i.e. the exfoliation of halloysite beginning from the inner layers, which is exploited to increase the lumen size. As a matter of fact, leaching requires extremely acid or alkaline conditions, as those realized by treating HNTs with H_2SO_4 from 1 to 6 M (Fu et al., 2017), or with NaOH 1 M at high temperature (McKerracher et al., 2012). Leaching is not considered in the present investigation.

[Figure 2 about here.]

3.1.1. Positively charged surfaces

The protonation and deprotonation of HNT was studied at different ionic strength by Bretti and co-workers (Bretti et al., 2016). They concluded that the

protonation constants increase accordingly to the ionic strength. Moreover, they run ζ-potential measurements as a function of pH in order to evaluate the HNT superficial charge. Accordingly, at pH = 2 both layers are protonated, from pH 2 to 6.5 the silicic surface undergoes deprotonation and at the highest point of the interval it reaches its lowest possible negative charge. The aluminic layer is protonated up to pH = 6 and then its deprotonation process is affected by the ionic strength. The data of Bretti and co-workers were useful in comprehending the thermodynamic of proton binding to HNT surfaces. Nevertheless the whole picture is still missing. Indeed, those data were collected from two separate systems representing the two layers of HNT, while in our model both surfaces are considered together.

Adding a proton on aluminic layer rather than on silicic one is only slightly discriminated from the energetic point of view, being the first process just -18.1 kJ mol^{-1} more exoergic than the second. On HNT(AlO-H) the proton is attached to the hydroxyl group while on HNT(SiO-H)to the oxygen between two silicon atoms. From the geometrical side, both HNT(AlO-H) and HNT(SiO-H) undergoes similar modifications, but they are less pronounced for the silic layer (Figure 3a,b). The two Si-O and Al-O bonds next to the attachment site are respectively +0.168/0.176 Å and 0.268A/0.300 Å longer with respect to the uncharged HNT. The other -OH groups on the Al layer orient their hydrogen atom as far as possible from the perturbation. The energy released (proton affinity) after the protonation of Si and Al layer is 983.5 and 1001.6 kJ mol^{-1}, respectively.

[Figure 3 about here.]

At extremely low pH value a second proton can be attached to the HNT surface sites. It could end up in three different positions and generates HNT(AlO-H/AlO-H,o,m,p) or their silicic analogous. As it can be easily foreseen, the most stable geometries are HNT(AlO-H/AlO-H,p) and HNT(SiO-H/SiO-H,p); thus only those two system geometries will be discussed here. The energy gap between HNT(AlO-H/AlO-H,p) and HNT(SiO-H/SiO-H,p) is more pronounced

than the one between the single protonated systems: HNT(AlO-H/AlO-H,p) is -49.3 kJ mol^{-1} more stable than HNT(SiO-H/SiO-H,p). When a second proton is added, the most significant geometry distortion is the further elongation of the neighbour Al-O and Si-O bonds, of 0.288/0.306 and 0.156/0.172 Åwith respect to HNT(AlO-H) and HNT(SiO-H) in the same order. It is worth noting that in the former system the presence of the second proton does not sensibly influence the geometry of the first one, while in HNT(SiO-H/SiO-H,p) the new H^+ makes the first one to reorient so that both of them look toward opposite directions (Figure 3c,d). This geometry difference could be the reason of the higher stability of HNT(AlO-H/AlO-H,p) over HNT(SiO-H/SiO-H,p), having the former the chance to better delocalize the extra positive charge. HNT(AlO-H/AlO-H,p) and HNT(SiO-H/SiO-H,p) protonation energies are -839.1 kJ mol^{-1} and -808.2 kJ mol^{-1} with respect to the monoprotonated system and -1840.7 and -1791.6 kJ mol^{-1} with respect to the uncharged HNT.

3.1.2. Negatively charged surfaces

The creation of a negative charge on the aluminic surface can be easily realized removing a proton. The Al-O bonds that insist on the deprotonated group shorten themselves by 0.096 and 0.104 Å, while the remaining hydroxyl group points toward the negative charge. This behaviour is just the opposite of the one obtained in HNT(AlO-H).

As anticipated, the creation of a negative charge on Si surface is not so straightforward as a simple proton removal (because there is no proton to remove). A possible path includes the formation of silanols via WMs reaction on surface, according to the following scheme (where the italic subscript on O is the number of HNT oxygen atoms bounded to Si):

(1) HNT-(O_{3}-Si-O-Si-O_{3}-)-HNT + H_2O → HNT-(O_{3}-SiOH HOSi-O_{3}-)-HNT

(2) HNT-(O_{3}-SiOH HOSi-O_{3}-)-HNT → HNT-(O_{3}-SiOH HOSi-O_{2}-)-HNT

(3a) HNT-(O_{3}-SiOH HOSi-O_{2}-)-HNT + H_2O → HNT-(O_{3}-SiOH $(HO)_2$Si-O_{2}-)-HNT^- + H^+

(3b) HNT-(O_{3}-SiOH HOSi-O_{2}-)-HNT + OH^- → HNT-(O_{3}-SiOH $(HO)_2$Si-O_{2}-)-HNT^-

In step (1) a WM hydrolyses on silicic surface, generating two Si-OH groups. One Si-O bond on the inner layer breaks and rotates exposing the -Si^+ moiety towards the surface (2), where it reacts with a further WM (3a) or equivalently with a OH^- (3b). This process generates three Si-OH on the surface, possibly a proton which moves away from the system in virtue of the basic environment and a negative charge delocalized on the silicic surface. As evaluated in (Fu et al., 2017), step (1) would require more than 200 kJ mol^{-1} of energy, but according to our calculations the global process which starts from HNT + H_2O + OH^- to produce HNT(Si-OH) would release 467.3 kJ mol^{-1}.

The geometries of HNT(Si-OH) and HNT(AlO^-) are reported in Figure 4a,b. The energy required for the negative charge formation on aluminic surface is 1374.9 kJ mol^{-1}, while 1358.8 kJ mol^{-1} are required for the whole HNT + $2H_2O \rightarrow$ HNT(Si-OH)+ H^+ process. Then, from a purely energetic point of view, it is slightly preferred that the negative charge is carried by this latter surface.

[Figure 4 about here.]

A second and a third deprotonation were studied on aluminic layer. HNT(AlO^{2-}) creation requires further 1654.3 kJ mol^{-1} with respect to the mono-negatively charged system, and HNT(AlO^{3-}) others 1854.4 kJ mol^{-1} respect to HNT(AlO^{2-}). Their geometries are reported in Figure 4c,d. The Al-OH groups subsequently de-protonated in HNT(AlO^{2-}) and HNT(AlO^{3-}) reacts in the same way as HNT(AlO^-): the Al-O bonds shorten themselves, by 0.184 and 0.144 Å in the former case and by 0.135 Å and 0.148 Å in the latter.

3.1.3. Dipole across the arms of HNT

Considering the data from the previous sections, there are two possible ways to create a charge separation: the first is making the Al surface negative and the Si one positive, namely HNT(AlO^-/SiO-H). The second is the other way around, HNT(AlO-H/Si-OH). The energies required to create these two kinds of across-the-arms dipoles are 226.0 and 202.6 kJ mol^{-1}, respectively. Again, a

negative charge is better carried by the silicic layer, as well as a positive charge formation preferably occurs on the gibbsitic surface. There are four possible negative-positive charge reciprocal positions with respect to the oxygen atoms hexagon of the latter surface, the usual -o, -m and -p plus the one referring to the same position, called -ipso (-i). It resulted that the -i configuration, reported in Figure 5a, is the most stable arrangememt for HNT(AlO^-/SiO-H). Conversely, HNT(AlO-H/Si-OH,p) is the most stable form for the second dipole geometry (Figure 5b). Since the only configuration treated will be HNT(AlO^-/SiO-H,i) and HNT(AlO-H/Si-OH,p), the symbol after the comma is no longer necessary and will be suppressed. From a geometrical point of view, the system response to a charge separation on one layer is basically the same as if there is no opposite charge on the other.

[Figure 5 about here.]

3.1.4. Positive or negative charge on both HNT sides

In the previous section the systems with opposite charges on the HNT surface were introduced, while here a description on HNT surfaces with same charge is presented (Figure 6). Such systems could exist when the pH environment is definitely acidic or alkaline. The doubly protonated system HNT(AlO-H/SiO-H) formation releases 1793.7 kJ mol^{-1}, while the doubly negatively charged system HNT(AlO^-/Si-OH) requires 2927.8 kJ mol^{-1}. Those two values should be compared with the sum of the protonation on both isolated HNT layers or with the sum of HNT(Si-OH) and HNT(AlO^-). The HNT(AlO-H/SiO-H) system accounts for the 90% of the sum of HNT(AlO-H) and HNT(SiO-H), while the 107% of the sum of HNT(Si-OH) and HNT(AlO^-) is required for HNT(AlO^-/Si-OH) formation. Thus it seems that the presence of a charge on one layer does influence the formation of a charge of the same sign on the other layer from an energetically point of view.

[Figure 6 about here.]

3.2. Water adsorption

Water adsorption on pristine halloysite was previously studied with different computational approaches on various model systems, see (Ferrante et al., 2017) and references therein. It is to remember that the model used in the present investigation allows to retain the geometrical effects due to the curvature of HNT surfaces, differently from other studies that can be found in the literature, which, albeit performed with similar methodologies, were based on models of flat kaolinite/gibbsite surfaces.

Before discussing WM adsorption on charged HNT Si and Al surfaces, the results we obtained on uncharged HNT are reported in order to make a coherent comparison. All calculated adsorption energies are reported in Table 1. Some adsorption geometries on positively charged silicic layer involve the formation of the H_3O^+ species on surface; in Table 1 these systems are marked with an asterisk.

[Table 1 about here.]

3.2.1. Adsorption on silicic layer

Two adsorption geometries were found for water on silicic layer. In the first one (mode I, Figure 7a), the WM acts as donor of two hydrogen bonds (which can considered as secondary interactions) with O atoms of the silicic ring and as acceptor of one relatively strong H-bond from a hydrogen belonging to the aluminic interlayer, with parameters O-HO(1.948,167). The computed interaction energy is -16.0 kJ mol^{-1}. The interaction with the interlayer disappears in presence of a second WM (Figure 7b). Now the first WM has a double donor interaction with the surface and an acceptor H-Bond with the second WM. The second WM interacts with silicon at a Si-O distance of 2.165 Å and stands almost parallel to the surface. The energy gain for the adsorption of one WM onto W-Si showing mode I adsorption, is -25.7 kJ mol^{-1}. As it can be expected, the surface adsorption of a WM facilitate the adsorption of other WMs.

[Figure 7 about here.]

The other adsorption geometry (mode II) for the WM in W-Si is entirely on the surface. This W-Si configuration (Figure 7c) shows two donor H-bonds with oxygen atoms that are in para position to each other and the interaction energy is -11.1 kJ mol^{-1}, which is lower than that of mode I adsorption. Adding a second WM leads to a similar geometry to the previously described W_2-Si, reported in Figure 7d. Now the first WM forms a three-way donor H-bond, including another superficial oxygen atom, plus the already known acceptor H-bond from the second. The interaction distance, 2.175 Å, from the silicon atom of the latter is slightly longer than the previous case. Still, the second WM lies parallel to the surface and its adsorption energy is -35.0 kJ mol^{-1}. Due to the presence of the extra donor H-bond from the first WM, this configuration is sensibly more stable than the one derived from the mode I W-Si geometry.

In conclusion, on silicic surface the water adsorption is a slightly exoergic process. It is worth noting that the formation of a Si-O_{water} interactions happens only in presence of (at least) two WM. Beside that, the second WM adsorption is more exoergic than the first one, which would mean that the WM single adsorption promotes further adsorptions.

3.2.2. Adsorption on positively charged silicic layer

The presence of H^+ on the W-SiO-H system does not allow the WM to interact with the inner HNT layer; the calculated adsorption energy is 129.7 kJ mol^{-1}. The WM extirpates the proton from the surface and adopts a three-fold-H-bond bridge configuration, as shown in figure 8a. In a more acidic environment, the WM in W-SiO-H/SiO-H,p does not form H_3O^+ and it loses the third interaction whit the superficial oxygen atom. As a result only one H-bond as acceptor and one as donor are revealed (Figure 8c), with an energy gain of only 78.6 kJ mol^{-1}.

It appears clear that the formation of the species H_3O^+ is far more convenient than simple H-bond interactions. When a second WM is added to the previous systems the H_3O^+ formation takes place in both scenarios. In W_2-SiO-H one of the three donor H-bonds with the surface is turned into one with the

WM of the same nature (Figure 8b). The adsorption energy is 41.0 kJ mol^{-1}. The decrease in the Δ_{ads} respect to W-SiO-H confirms the hypothesis that the interaction of H_3O^+ with the surface is more favourable than the one with another WM. As a matter of fact, the adsorption geometry in W_2-SiO-H/SiO-H,p shows two H_3O^+ on different adsorption sites (Figure 8d), so that two three-fold-H-bond bridges are formed, with a calculated adsorption energy of 185.7 kJ mol^{-1}, which is a value higher than the ones from both W-SiO-H/SiO-H,p and W-SiO-H. The reason is easy to understand in the latter case. It is considered an energetically more convenient adsorption geometry the one that includes an interaction with the surface rather than with a WM. The extra energy gain with respect to W-SiO-H could find explanation in a more extended charge spreading over the silicic layer.

[Figure 8 about here.]

3.2.3. Adsorption on negatively charged silicic layer

The interaction energy of a WM with the negatively charged silicic surface is equal to 60.4 kJ mol^{-1}. WM forms an acceptor H-bond with the silanol group -SiOH and two as donor with the superficial oxygen atom, one of which is a secondary interaction (Figure 9a). A second WM adsorption releases further 35.1 kJ mol^{-1}. The already present WM does not change too much its adsorption geometry, with one acceptor and two donor H-bonds. Also the second WM shows the same number and type of interactions: it has one H-bond as acceptor with the -SiOH group and two as donor: one with the first WM and the other with a superficial oxygen atom. This geometry is reported in Figure 9b. Despite the same number and type of interactions are present in W-Si-OH and W_2-Si-OH, the latter has a lower adsorption energy with respect to the former. Moving from W-Si-OH to W_2-Si-OH, the only appreciable difference in the first WM adsorption geometry is the increasing of the H-bond angle with the -SiOH group. This fact cannot explain the energy difference on its own, hence we could conclude that, also in presence of a negative charge, one H-bond between WMs

is less convenient than one between WM and the surface.

[Figure 9 about here.]

3.2.4. Adsorption on aluminic layer

On aluminic surface there is only one adsorption geometry. The calculated adsorption energies are 52.2 and 36.9 kJ mol^{-1} for W-Al and W_2-Al, respectively. In the first system the WM forms one H-bond as donor with the surface and one as acceptor, plus a secondary H-bond as acceptor. The hydrogen atom not involved in the surface interactions faces the inner part of the nanotube (Figure 10a). In W_2-Al the first WM loses its secondary acceptor H-bond, remaining with only one H-bond as acceptor and one as donor. The second WM has one H-bond as acceptor with the superficial -OH group previously involved in the secondary interaction in W-Al and one H-bond as donor with the surface. The second WM hydrogen atom that does not participate in any interaction lays parallel to the surface. The optimized geometry is reported in Figure 10b. The energy gain in W_2-Al is around 71% respect to W-Al. The trend is opposite to the one found in the silicic surface, where the adsorption of the first WM releases less energy than the adsorption of the second.

[Figure 10 about here.]

3.2.5. Adsorption on positively charged aluminic surface

The water adsorption energy in W-AlO-H is 69.9 kJ mol^{-1}. Despite the net charge, the adsorption geometry (Figure 11a) is not too different from the one in W-Al: a donor H-bond and an acceptor one from the protonated -OH group. The higher energy gain is obviously due to the latter interaction. Also in W_2-AlO-H the adsorption geometry (Figure 11b) is similar to the W_2-Al one. The second WM stays in front of the first one and interacts with the uncharged -OH group. The adsorption on two different sites is preferred over an H-bond extended network creation. The second WM behaves as if it is the only one

on the surface as confirmed by a calculated adsorption energy for W_2-AlO-H of 54.1 kJ mol^{-1}, which is very close to the energy computed in W-Al. In W_2-AlO-H the first WM forms an acceptor H-bond with the protonated -OH group and one as donor, like in the W-AlO-H scenario. Also the second WM has an acceptor-donor interaction with the surface, but with regular hydroxyl group. Both of the WMs keep the hydrogen atom not involved in the H-bond perpendicular to the surface. Unlike the silicic layer, the surface is not able to donate its proton to the WM, thus there is no H_3O^+ formation on aluminic layer.

In a more acidic environment, the WM in W-AlO-H/AlO-H,p system seems to be immune to the the presence of another proton. As a matter of fact, this system shows similar Δ_{ads}, -66.9 kJ mol^{-1}, and geometry of W-AlO-H: one acceptor and one donor H-bond. Its geometry is shown in Figure 11c. When a second WM is added to W-AlO-H/AlO-H,p, an H-bond network takes place, involving the non protonated adjacent ring (Figure 11d). The first WM has a donor H-bond and one as acceptor from the protonated -OH group. The second WM has one acceptor (from the first WM) and a donor H-bond. The computed adsorption energy for W-AlO-H/AlO-H,p is 65.7 kJ mol^{-1}.

[Figure 11 about here.]

3.2.6. Adsorption on negatively charged aluminic surface

The proton removed from the HNT aluminic layer is the one facing the center of the Al-O ring. Despite the presence of an unsaturation, in W-AlO^- the surface has not the strength to remove a proton from H_2O. Thus the WM has a donor-acceptor H-bond bridge with the deprotonated hydroxyl group. When a second WM is adsorbed, the geometry of the first one is not sensibly changed: the same donor-acceptor H-bond bridge are observed, while the other WM forms a double donor and a single acceptor H-bond with a different -OH group. The adsorption geometries for W-AlO^- and W_2-AlO^- are reported in Figure 12a,b. The calculated adsorption energies are 75.5 kJ mol^{-1} and 59.2 kJ mol^{-1} for

W-AlO$^-$ and W$_2$-HNT(AlO$^-$) respectively. The interaction with the charged site rather than a neutral one releases more energy, as it is suppose to happen. Nevertheless, the second WM geometry with its triple H-bond ensures a high energy gain, more pronounced than the one computed in the simple W-Al.

[Figure 12 about here.]

Removing a further proton from HNT aluminic layer leads to an adsorption energy of 110.9 and 72.7 kJ mol^{-1} for W-AlO^{2-} and W$_2$-AlO^{2-} respectively. The stronger adsorption in W-AlO^{2-} respect to W-AlO$^-$ can be due to the interaction of the WM with two deprotonated groups in place of only one. In particular, there are two donor H-bonds with the negatively charged hydroxyl groups and one acceptor H-bond with the -OH group in meta position. In W$_2$-AlO^{2-} the first WM retains its previously described interactions, while the second WM acts as H-bond donor toward the first WM and the surface, and also as H-bond acceptor from a superficial hydroxyl group. The formation of such complex H-bond network remarkably lowers the system energy. The optimized adsorption geometries for W-AlO^{2-} and W$_2$-AlO^{2-} are shown in Figure 12c-d.

In the HNT(AlO^{3-}) surface, finally, the adsorption energy for one and two water molecules are respectively 93.5 and 114.1 kJ mol^{-1}. The higher Δ_{ads} of W-AlO^{3-} with respect W-AlO^{2-} is likely due to the missing interaction with the third deprotonated hydroxyl group, which instead interacts with the second WM in W$_2$-AlO^{3-} and increase the adsorption strength (Figure 12f). The first WM participates in a donor H-bond with two of them and the second WM with the last. The remaining interactions are those between water molecules, where the first WM acts as acceptor, and a further acceptor H-bond formed by the second WM with the surface.

3.2.7. Effect of a charge on the opposite HNT layer

This section is devoted to answer the question: can a superficial modification on one site of the halloysite affect the adsorption on the other? In order to obtain this information, the optimized geometries computed for the uncharged systems

have been modified creating a charge on the opposite layer and reoptimized.

[Table 2 about here.]

In the outer HNT surface the adsorption geometries are almost identical to those found in the uncharged HNT but an analogous consideration is not true from the energetic point of view. As a matter of fact, the adsorption energies, reported in Table 2, are sensibly influenced by the charge on the opposite layer and the orientation of the WM on HNT plays a fundamental role on this effect. If the perturbation on the opposite layer has a sign opposite to the dipole on WM, then the system energies are lowered. This is the case of the adsorption of one WM on the silicic layer. In the mode I geometries, the WM dipole positive end points at the inner layer, in order to interact with the hydroxyl group. Thus a positive charge on the Al layer lowers the system energy, while deprotonating the opposite layer causes a small destabilization. The reverse situation occurs in the single water adsorption mode II, in which the WM is twisted with respect to the previous case. In the adsorption of two WMs on silicic surface the perturbations suffered by the H-bond are negligible in the geometry reached starting from mode I geometry, probably due to the presence of Si-O interaction. A slightly different situation occurs when the second WM is added to mode II configuration. In this case, the Si-O distance elongates (by 0.061 Å) or shortens (by 0.064 Å) itself respectively when a proton is removed or added to the aluminic layer, while the other H-bond parameters do not change significantly. In the adsorption of the second WM on the silicic layer of HNT(AlO-H), the first WM moves from a situation in which its dipole positive portion points toward the aluminic charged surface, to a more convenient orientation. The Si-O distance shortening and the latter factor contribute to lowering the system energy.

In the aluminic layer, the water molecule dipole lays almost parallel to the surface. Thus the influence of a charge is not as predictable as in the adsorption on the silicic surface. In particular the single WM adsorption on the inner HNT layer of HNT(Si-OH) system has a lower Δ_{ads} energy than the one on

HNT. Despite the adsorption geometries look very similar to each other, on the negatively charged surface the WM H-bonds are definitely better oriented. All the H-bond distances are shorter and one secondary interaction is promoted to regular H-bond: in detail, O-HO(1.946,164.5), O-HO(1.959,155.4) and OH-O(1.667,156.7). The perturbation allows the WM to get closer to the HNT aluminic surface, lowering the system energy. In the case of a double WM adsorption on the uncharged HNT, the second WM "steals" the secondary H-bond as donor from the first to create a regular H-bond of the same nature with the second WM. In that configuration, both WMs have a donor-acceptor H-bond bridge with the surface, even if they are differently oriented. The negative charge on the silicic layer forces the second WM to change its orientation on the HNT surfaces by making the second WM dipole point in the same direction as the first WM (Figure 13). This way the first WM maintains its donor-acceptor bridge with the surface and the second WM acquires a further H-bond as acceptor involving another hydroxyl group, while the one used in W_2-Al as donor H-bond provider becomes an H-bond acceptor. Not surprisingly, from an energetic point of view, the single WM adsorption on HNT(SiO-H) aluminic layer shows an opposite trend respect to the HNT(Si-OH) case. While the characteristics of the H-bonds as acceptor (both primary and secondary) from the surface are not so different, the H-bond as donor is 0.05 Å longer, which determines a weaker interaction. Adding a second WM to the previous system restores the geometry of the uncharged system and so the energy.

[Figure 13 about here.]

3.2.8. Adsorption on HNT surface in presence of a dipole

There are two possible ways to form a dipole on HNT. When the negative charge is on the aluminum layer and the positive one on the silicic surface, the adsorption geometries for both one and two WM on both sides of HNT do not show sensible variations with respect presented in absence of dipole. In fact, W-(Al)-AlO^-/SiO-H adsorption geometry has an acceptor-donor H-bond

bridge that involves the deprotonated -OH group, O-HO(1.777,154.2) and OH-O(1.533,165.8), with a Δ_{ads} of 78.1 kJ mol^{-1}. In W-(Si)-AlO$^-$/SiO-H the H_3O^+ species is generated on surface and forms three donor H-bond: OH-O(1.637,169), OH-O(1.731,173) and OH-O(1.725,177). The Δ_{ads} is -130.0 kJ mol^{-1}. When a second WM is added the on Al negatively charged layer, the acceptor-donor H-bond bridge is still observed, O-HO(1.770,156.5) and OH-O(1.551,167.0) and the second WM forms one acceptor H-bond with the former, O-HO(2.302,129). In turn, the second WM forms a further acceptor-donor H-bond bridge with the -OH group in ortho position from the deprotonated site, O-HO(1.954,153) and OH-O(1.805,161). Despite the geometry is quite similar, the energy gain is slightly lower than W_2-AlO$^-$: -49.5 kJ mol^{-1}. On the silicic surface, W_2-(Si)-AlO$^-$/SiO-H adsorption geometry has two donor H-bonds from H_3O^+, OH-O(1.691,174) and OH-O(1.743,171), which forms a further H-bond as donor with the second WM, OH-O(1.457,176). The second WM forms an H-bond with the surface, OH-O(1.830,154). This latter interaction is the difference between W_2-(Si)-AlO$^-$/SiO-H and W_2-HNT(SiO-H) from a geometrical point of view. Nevertheless the energy gain is similar to the one calculated on absence of dipole: -45.6 kJ mol^{-1}.

Another possible dipole configuration on HNT surface can be realized when a proton is attached on the aluminic layer of the system HNT(Si-OH). With respect to the first dipole formation scenario, here there are some differences in water adsorption geometries. The Δ_{ads} computed from W-(Al)-AlO-H/Si-OH is slightly lower (-74.6 kJ mol^{-1}) than the W-AlO-H one. The reason could be ascribable to a more symmetrical adsorption geometry of the WM on the aluminic layer. While on W-AlO-H the WM acts as H-bond donor in -ortho and -meta positions, here a double H-bond as donor with both -ortho -OH groups is present (Figure 14a). The WM also has an acceptor H-bond from the protonated -OH group. Unlike what happens on aluminic layer, on the silicic one the adsorption geometry and energy are similar to the W-Si-OH one. The Δ_{ads} is almost identical: -60.8 kJ mol^{-1}. The computed interactions are two donor H-bonds toward the surface and one as acceptor for the silanolic group,

as reported in Figure 14c). Adding a second WM on alluminic surface leads to an energy gain of 27.6 kJ mol^{-1}. The first WM keeps its geometry with one acceptor H-bond from the protonated -OH and a double donor H-bond. The second WM has one as donor and two as acceptor H-bond. This systems geometry is reported in Figure 14b. In the silicic surface a second WM only slightly changes the adsorption geometry of the first (Figure 14d). The already present WM forms two H-bonds as donor and one as acceptor from the -SiOH group. The second WM forms a donor H-bond with the first one, an acceptor with another superficial -SiOH group and one as donor with the superficial oxygen atom. The adsorption energy is -36.9 kJ mol^{-1}.

[Figure 14 about here.]

3.2.9. Adsorption on both silicic and aluminic surfaces positively charged

On Al layer of HNT(AlO-H) the modifications on the silicic surface do not affects sensibly the single WM adsorption geometries. In particular, W-(Al)-AlO-H/SiO-H shows an acceptor-donor H-bond bridge, see Figure 15a, just as in the W-AlO-H system. The calculated Δ_{ads} is -75.4 kJ mol^{-1}. The same conclusion is not applicable to W_2-(Al)-AlO-H/SiO-H: here the second WM interacts with the already present species rather than with the surface (Figure 15b). In detail, the first WM has the usual acceptor-donor H-bond bridge plus a donor H-bond with the second WM. As a consequence, the adsorption energy is less pronounced with respect to the W_2-AlO-H system: -46.7 kJ mol^{-1}, confirming that the interaction with the surface is preferred over the one between water molecules. When the single and double water adsorptions occur on silicic surface ((Figures 15c,d)) the geometries are quite similar to W-SiO-H and W_2-SiO-H, but the Δ_{ads} are lower: -164.6 in W-(Si)-AlO-H/SiO-H and -59.1 kJ mol^{-1} in W_2-(Si)-AlO-H/SiO-H. The reason for such differences should lie in a H-bond angle more close to 180° in W-(Si)-AlO-H/SiO-H if compared to W-SiO-H and in a shorter H-bond distances in W_2-(Si)-AlO-H/SiO-H with respect to W_2-SiO-H. The H_3O^+ species generated in W-(Si)-AlO-H/SiO-H forms the

usual three donor H-bond, while in W_2-(Si)-AlO-H/SiO-H the protonated WM forms only two H-bonds as donor with the surface, and another one with the second WM, which in turn, has a donor H-bond with the surface.

[Figure 15 about here.]

3.2.10. Adsorption on both silicic and aluminic surfaces negatively charged

W-(Al)-AlO^-/Si-OH adopts a geometry similar to W-AlO^- (Figure 16a). Here an acceptor-donor H-bond bridge can be found, which involves the deprotonated hydroxyl group. The computed adsorption energy is similar to the aforementioned system: -80.5 kJ mol^{-1}. In W_2-(Al)-AlO^-/Si-OH the first WM acceptor H-bond is downgraded to secondary interaction while the donor one is maintained. The second WM has a donor H-bond interaction with the first one and with the oxygen atom in meta position respect to the deprotonated group, plus an acceptor H-bond with the one in ortho position. The computed Δ_{ads} is -83.2 kJ mol^{-1} and the optimized geometry is reported in Figure 16b. For both W-(Al)-AlO^-/Si-OH and W_2-(Al)-AlO^-/Si-OH the adsorption energies are lower than the ones computed in W-AlO^- and W_2-AlO^-, despite their geometries are similar to the system where there is no negative charge on silicic surface. On the opposite HNT layer, the geometric and energetic differences between W-(Si)-AlO^-/Si-OH or W_2-(Si)-AlO^-/Si-OH with the simpler adsorption on HNT(Si-OH) system are more pronounced (Figure 16c,d). In W-(Si)-AlO^-/Si-OH, the WM is able to interact with two silanolic groups; it forms an acceptor H-bond with one of them, in an analogous way to W-Si-OH. The second silanolic H-bond has a donor nature and a further H-bond as donor with an oxygen atom bonded to two silicon ones is added to the silanolic interaction. The ability to involve two -SiOH groups (and not just one like in W-Si-OH) increases the adsorption energy to 114.3 kJ mol^{-1}. In W_2-(Si)-AlO^-/Si-OH the first WM adsorption mode is similar to W-(Si)-AlO^-/Si-OH: two donor H-bonds are present, one with the oxygen atom linked to two silicon ones and the other toward a silanolic group. The second WM only has a single donor H-bond

with the first one. The adsorption energy is -33.9 kJ mol^{-1}, a value compatible with the one calculated when the second WM interacts with just the already present one.

[Figure 16 about here.]

4. Conclusion

The computational investigation of halloysite nanotube structural forms at different pH was performed on a portion cropped from a periodic HNT model, which was modified by creating different superficial charges. The energetic aspects of these processes were evaluated and the informations collected allowed to determine the stability order of the HNT structures when some charges are present on its layers. It turns out that the preferred protonated site in acidic chemical environment is the aluminic surface which is slightly more stable than the silicic counterpart. At the lowest pH values, three possible scenarios could appear: a double protonation on aluminic or silicic layer and a single protonation on both the HNT surfaces. The double protonated aluminic layer system is the most energetically favoured among the three. The double protonated silicic layer occupies the second position in the stability order, being slightly more stable than the system in which both layers are protonated once. In other words, in case that the first protonation occurs on the alluminic layer in a mild acid environment, the second protonation will follow on the same side if the pH is lowered. On the other hand, in the case where the first proton was attached on the silicic side at mild acidic pH, the second protonation can occur both on silicic or alluminic layer, with very similar energetic aspects, in strong acidic environment. The most stable system with opposite charges on the HNT surface shows a positive charge on the aluminic layer and a negative charge on the silicic one. The negative charge formation happens via the creation of silanolic groups after the reaction of the surface with water molecules in alkaline conditions. The other dipole configuration sees the HNT layers carrying a charge of opposite

sign with respect to the aforementioned system. In a mild alkaline environment a negative charge could be present on one HNT layer and this phenomenon occurs most likely on the silicic layer via silanol formation rather than through the deprotonation of the aluminic layer. Keep raising the pH value, a double negative charge is better handled by the HNT system sharing the extra charge on both surfaces.

Moving forward, the modification of the halloysite surface through pH changes is a process exploited in a number of HNT-nanomaterial synthesis. The molecules of interest are required to interact with charged HNT surfaces in presence of water, so the investigation on the adsorption of WMs on HNT surface lays the groundwork for any other study on HNT-nanocomposite synthesized at non-neutral pH environment. The WM does not have a preferential layer of adsorption valid for every HNT modified structure. The formation of the H_3O^+ species on the positively charged silicic layer makes the systems in which it is present far more stable than their analogous version on aluminic layer. The stabilization provided by the H_3O^+ formation, but also the WMs adsorption itself, could reverse stability order of the anhydrous HNT. In neutral pH environment, the gibbsitic surface shows more pronounced adsorption energies due to the formation of hydrogen bonds networks. Raising the pH value or in presence of a dipole across the spiral arms, the stability order has to be determined on a case-by case basis. A recurrent event is recorded according to the investigation: in system where two water molecules are adsorbed on surface, the second WM rather binds to the surface instead of interacting with the already present WM, even if this behaviour prevents the occuring of any interactions between them. In the end, the effect of a charge of the opposite layer on the adsorbed WM has been investigated. It turns out that this phenomenon can actually provoke some important changes in the WM adsorption energy, hence could have a role in the tuning capacity of the HNT inner lumen and on the interlayer spacing occurring in different pH environments.

References

Abdullayev, E., Joshi, A., Wei, W., Zhao, Y., & Lvov, Y. (2012). Enlargement of halloysite clay nanotube lumen by selective etching of aluminum oxide. *ACS nano*, *6*, 7216–7226.

Anastopoulos, I., Mittal, A., Usman, M., Mittal, J., Yu, G., Núñez-Delgado, A., & Kornaros, M. (2018). A review on halloysite-based adsorbents to remove pollutants in water and wastewater. *Journal of Molecular Liquids*, *269*, 855–868.

Bertolino, V., Cavallaro, G., Lazzara, G., Milioto, S., & Parisi, F. (2017). Biopolymer-targeted adsorption onto halloysite nanotubes in aqueous media. *Langmuir*, *33*, 3317–3323.

Boys, S., & Bernardi, d. F. (1970). The calculation of small molecular interactions by the differences of separate total energies. some procedures with reduced errors. *Molecular Physics*, *19*, 553–566.

Bretti, C., Cataldo, S., Gianguzza, A., Lando, G., Lazzara, G., Pettignano, A., & Sammartano, S. (2016). Thermodynamics of proton binding of halloysite nanotubes. *The Journal of Physical Chemistry C*, *120*, 7849–7859.

Eichkorn, K., Treutler, O., Öhm, H., Häser, M., & Ahlrichs, R. (1995). Auxiliary basis sets to approximate coulomb potentials. *Chemical physics letters*, *240*, 283–290.

Eichkorn, K., Weigend, F., Treutler, O., & Ahlrichs, R. (1997). Auxiliary basis sets for main row atoms and transition metals and their use to approximate coulomb potentials. *Theoretical Chemistry Accounts*, *97*, 119–124.

Fakhrullin, R., Tursunbayeva, A., Portnov, V., & L'vov, Y. M. (2014). Ceramic nanotubes for polymer composites with stable anticorrosion properties. *Crystallography Reports*, *59*, 1107–1113.

Fakhrullin, R. F., & Lvov, Y. M. (2016). Halloysite clay nanotubes for tissue engineering. *Nanomedicine*, *11*, 2243–2246.

Fakhrullina, G. I., Akhatova, F. S., Lvov, Y. M., & Fakhrullin, R. F. (2015). Toxicity of halloysite clay nanotubes in vivo: a caenorhabditis elegans study. *Environmental Science: Nano*, *2*, 54–59.

Ferrante, F., Armata, N., Cavallaro, G., & Lazzara, G. (2017). Adsorption studies of molecules on the halloysite surfaces: A computational and experimental investigation. *The Journal of Physical Chemistry C*, *121*, 2951–2958.

Ferrante, F., Armata, N., & Lazzara, G. (2015). Modeling of the halloysite spiral nanotube. *The Journal of Physical Chemistry C*, *119*, 16700–16707.

Frisch, M. J., Trucks, G. W., Schlegel, H. B., Scuseria, G. E., Robb, M. A., Cheeseman, J. R., Scalmani, G., Barone, V., Mennucci, B., Petersson, G. A., Nakatsuji, H., Caricato, M., Li, X., Hratchian, H. P., Izmaylov, A. F., Bloino, J., Zheng, G., Sonnenberg, J. L., Hada, M., Ehara, M., Toyota, K., Fukuda, R., Hasegawa, J., Ishida, M., Nakajima, T., Honda, Y., Kitao, O., Nakai, H., Vreven, T., Montgomery, J. J. A., Peralta, J. E., Ogliaro, F., Bearpark, M., Heyd, J. J., Brothers, E., Kudin, K. N., Staroverov, V. N., Kobayashi, R., Normand, J., Raghavachari, K., Rendell, A., Burant, J. C., Iyengar, S. S., Tomasi, J., Cossi, M., Rega, N., Millam, J. M., Klene, M., Knox, J. E., Cross, J. B., Bakken, V., Adamo, C., Jaramillo, J., Gomperts, R., Stratmann, R. E., Yazyev, O., Austin, A. J., Cammi, R., Pomelli, C., Ochterski, J. W., Martin, R. L., Morokuma, K., Zakrzewski, V. G., Voth, G. A., Salvador, P., Dannenberg, J. J., Dapprich, S., Daniels, A. D., Farkas, Ö., Foresman, J. B., Ortiz, J. V., Cioslowski, J., & Fox, D. J. (2009). Gaussian 09 Revision D.01. Gaussian Inc. Wallingford CT.

Fu, L., Yang, H., Tang, A., & Hu, Y. (2017). Engineering a tubular mesoporous silica nanocontainer with well-preserved clay shell from natural halloysite. *Nano Research*, *10*, 2782–2799.

Gaaz, T., Sulong, A., Kadhum, A., Al-Amiery, A., Nassir, M., & Jaaz, A. (2017). The impact of halloysite on the thermo-mechanical properties of polymer composites. *Molecules*, *22*, 838.

Guo, B., Lei, Y., Chen, F., Liu, X., Du, M., & Jia, D. (2008). Styrene-butadiene rubber/halloysite nanotubes nanocomposites modified by methacrylic acid. *Applied Surface Science*, *255*, 2715–2722.

Joussein, E., Petit, S., Churchman, J., Theng, B., Righi, D., & Delvaux, B. (2005). Halloysite clay minerals - a review. *Clay Minerals*, *40*, 383–426.

Lazzara, G., Cavallaro, G., Panchal, A., Fakhrullin, R., Stavitskaya, A., Vinokurov, V., & Lvov, Y. (2018). An assembly of organic-inorganic composites using halloysite clay nanotubes. *Current Opinion in Colloid & Interface Science*, *35*, 42–50.

Lin, Y., Ng, K. M., Chan, C.-M., Sun, G., & Wu, J. (2011). High-impact polystyrene/halloysite nanocomposites prepared by emulsion polymerization using sodium dodecyl sulfate as surfactant. *Journal of colloid and interface science*, *358*, 423–429.

Lisuzzo, L., Cavallaro, G., Parisi, F., Milioto, S., Fakhrullin, R., & Lazzara, G. (2019). Core/shell gel beads with embedded halloysite nanotubes for controlled drug release. *Coatings*, *9*, 70.

Lvov, Y., Wang, W., Zhang, L., & Fakhrullin, R. (2016a). Halloysite clay nanotubes for loading and sustained release of functional compounds. *Advanced Materials*, *28*, 1227–1250.

Lvov, Y. M., DeVilliers, M. M., & Fakhrullin, R. F. (2016b). The application of halloysite tubule nanoclay in drug delivery. *Expert opinion on drug delivery*, *13*, 977–986.

Lvov, Y. M., Shchukin, D. G., Mohwald, H., & Price, R. R. (2008). Halloysite clay nanotubes for controlled release of protective agents. *Acs Nano*, *2*, 814–820.

Massaro, M., Colletti, C., Lazzara, G., Milioto, S., Noto, R., & Riela, S. (2017). Halloysite nanotubes as support for metal-based catalysts. *Journal of Materials Chemistry A*, *5*, 13276–13293.

Massaro, M., Riela, S., Cavallaro, G., Colletti, C., Milioto, S., Noto, R., & Lazzara, G. (2016). Ecocompatible halloysite/cucurbit [8] uril hybrid as efficient nanosponge for pollutants removal. *ChemistrySelect*, *1*, 1773–1779.

McKerracher, R., Bavykin, D., & Walsh, F. (2012). The stability of halloysite nanotubes in acidic and alkaline aqueous suspensions. *Nanotechnology*, *23*, 065705.

Núñez-Delgado, A., Álvarez-Rodríguez, E., Fernández-Sanjurjo, M. J., Nóvoa-Muñoz, J. C., Arias-Estévez, M., & Fernández-Calviño, D. (2015). Perspectives on the use of by-products to treat soil and water pollution. *Microporous and Mesoporous Materials*, *210*, 199–201.

Papoulis, D. (2019). Halloysite based nanocomposites and photocatalysis: A review. *Applied Clay Science*, *168*, 164–174.

Pasbakhsh, P., Churchman, G. J., & Keeling, J. L. (2013). Characterisation of properties of various halloysites relevant to their use as nanotubes and microfibre fillers. *Applied Clay Science*, *74*, 47–57.

Prishchenko, D. A., VZenkov, E., Mazurenko, V. V., Fakhrullin, R. F., Lvov, Y. M., & Mazurenko, V. C. (2018). Molecular dynamics of the halloysite nanotubes. *Physical Chemistry Chemical Physics*, *20*, 5841–5849.

Rozza, R., Armata, N., Lazzara, G., Parisi, F., & Ferrante, F. (2019). Halloysite nanotubes and metal corrosion inhibitors: a computational and experimental study. *The Journal of Physical Chemistry C*, *97*, 119–124.

Schäfer, A., Horn, H., & Ahlrichs, R. (1992). Fully optimized contracted gaussian basis sets for atoms li to kr. *The Journal of Chemical Physics*, *97*, 2571–2577.

Shchukin, D. G., Lamaka, S., Yasakau, K., Zheludkevich, M., Ferreira, M., & Möhwald, H. (2008). Active anticorrosion coatings with halloysite nanocontainers. *The Journal of Physical Chemistry C*, *112*, 958–964.

Vergaro, V., Abdullayev, E., Lvov, Y. M., Zeitoun, A., Cingolani, R., Rinaldi, R., & Leporatti, S. (2010). Cytocompatibility and uptake of halloysite clay nanotubes. *Biomacromolecules*, *11*, 820–826.

Wang, Q., Wang, Y., Zhao, Y., Zhang, B., Yunyin, N., Xiang, X., & Chen, R. (2015). Fabricating roughened surfaces on halloysite nanotubes via alkali etching for deposition of high-efficiency pt nanocatalysts. *CrystEngComm*, *17*, 3110–3116.

White, R. D., Bavykin, D. V., & Walsh, F. C. (2012). The stability of halloysite nanotubes in acidic and alkaline aqueous suspensions. *Nanotechnology*, *23*, 065705.

Yuan, P., Tan, D., & Annabi-Bergaya, F. (2015). Properties and applications of halloysite nanotubes: recent research advances and future prospects. *Applied Clay Science*, *112*, 75–93.

Zhang, A., Pan, L., Zhang, H., Liu, S., Ye, Y., Xia, M., & Chen, X. (2012). Effects of acid treatment on the physico-chemical and pore characteristics of halloysite. *Colloids and Surfaces A: Physicochemical and Engineering Aspects*, *396*, 182–188.

Zhao, Y., & Truhlar, D. G. (2006). A new local density functional for main-group thermochemistry, transition metal bonding, thermochemical kinetics, and noncovalent interactions. *The Journal of chemical physics*, *125*, 194101.

List of Figures

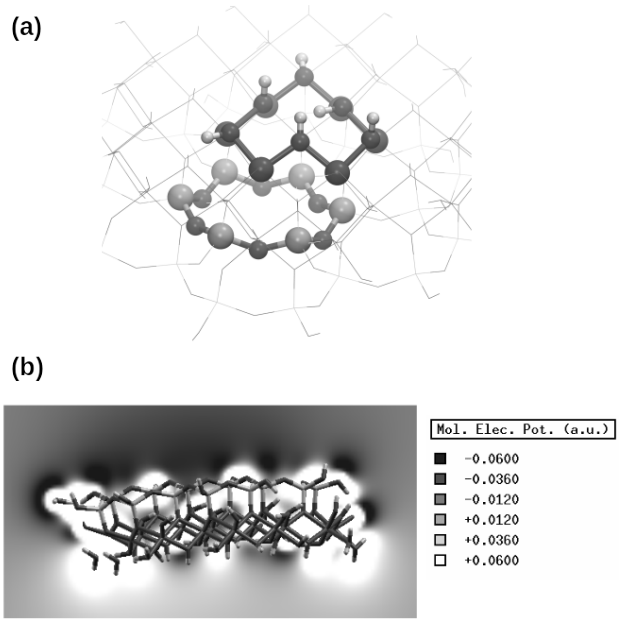

Figure 1: (a) The HNT model used in this work. The silicic and aluminic surface portions involved in charge modifications and adsorption of water molecules are ball-and-stick highligthed and the remainder of the system is in wireframe representation; see (Ferrante et al., 2017) for a full picture. (b) The molecular electrostatic potential (a.u.) map, calculated according to the method used in this work, in a plane crossing perpendicularly the center of the HNT model and containing the nanotube axis.

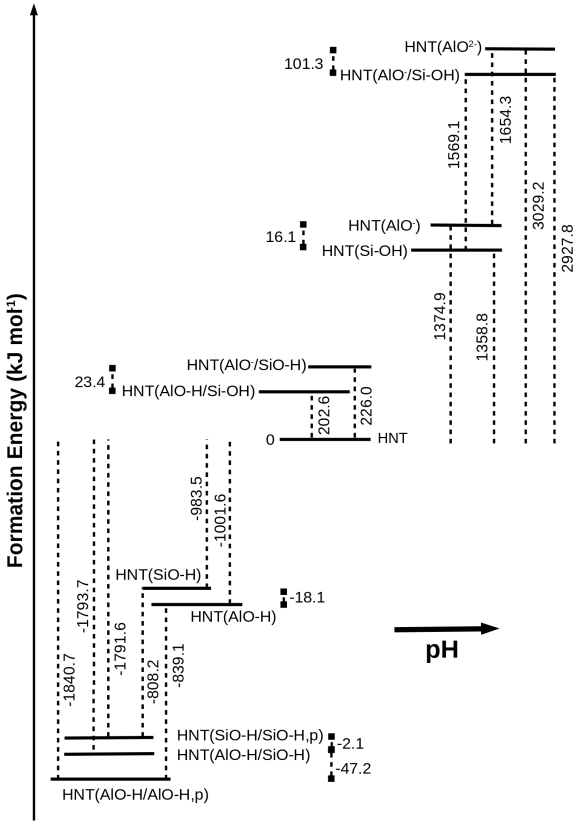

Figure 2: Energetics of the possible HNT systems at different pH conditions. Energy differences are reported in kJ mol^{-1} and are not in scale.

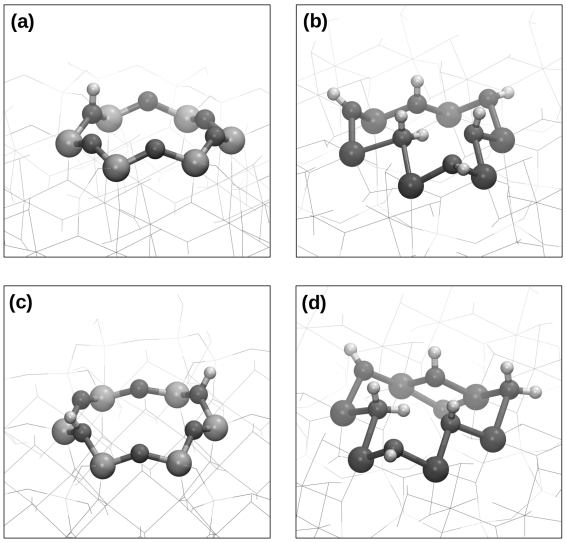

Figure 3: Optimized geometries of (a) HNT(SiO-H) (b) HNT(AlO-H) (c) HNT(SiO-H/SiO-H,p) and (d) HNT(AlO-H/AlO-H,p).

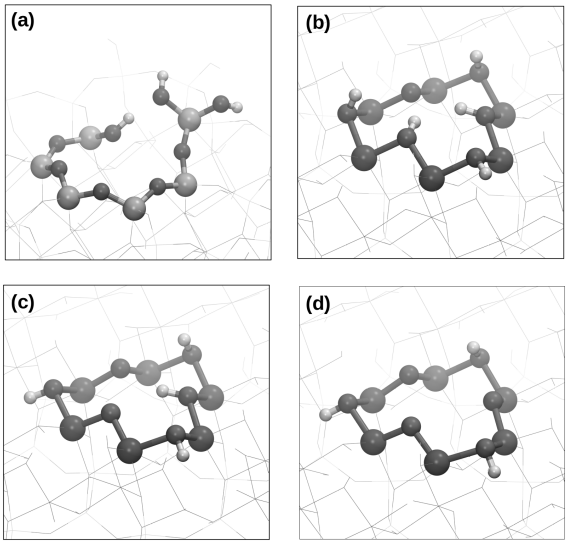

Figure 4: Optimized geometries of (a) HNT(Si-OH) (b) HNT(AlO^{-}), (c) HNT(AlO^{2-}) and (d) HNT(AlO^{3-}).

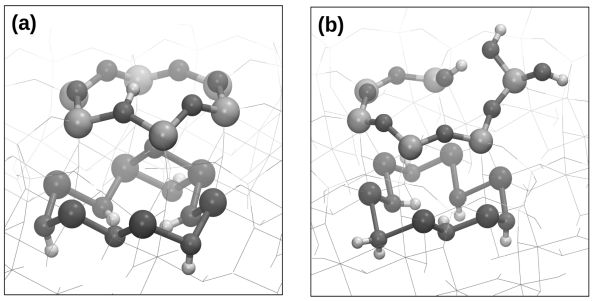

Figure 5: (a) HNT(AlO^-/SiO-H,i) and (b) HNT(AlO-H/Si-OH,p) optimized geometries.

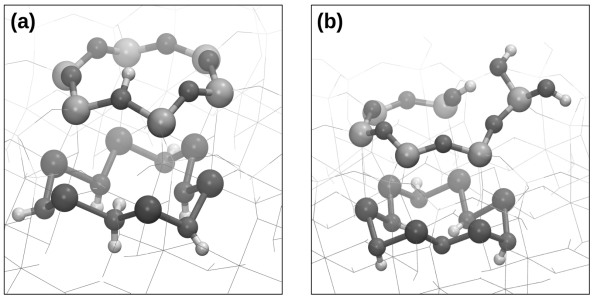

Figure 6: (a) HNT(AlO-H/SiO-H) and (b) HNT(AlO^-/Si-OH) optimized geometries.

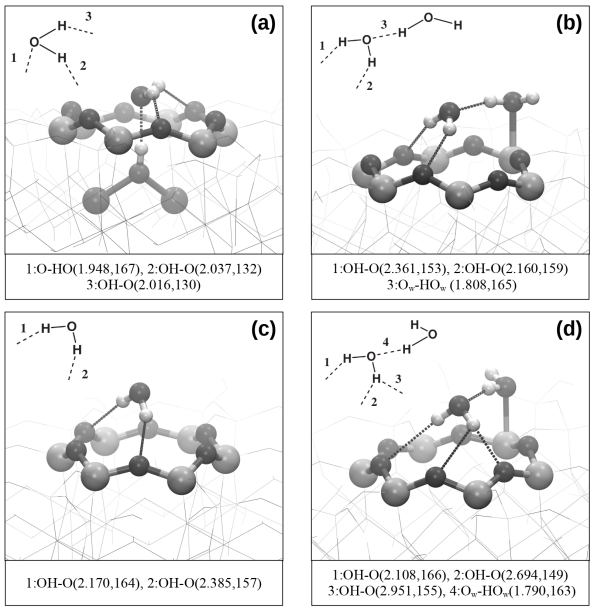

Figure 7: Optimized adsorption geometries of the systems with one (a) or two (b) WMs on the silicic surface in the mode I configuration, and with one (c) or two (d) water molecules in the mode II configuration. Hydrogen bonds parameters are reported in the insets.

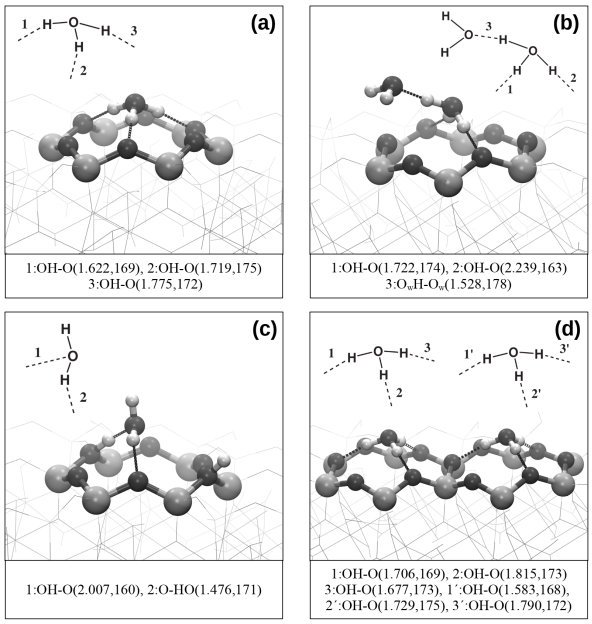

Figure 8: Optimized adsorption geometries of one (a) or two (b) WMs on the HNT(SiO-H) surface and one (c) or two (b) WMs on the HNT(SiO-H/SiO-H,p) surface. Hydrogen bonds parameters are reported in the insets.

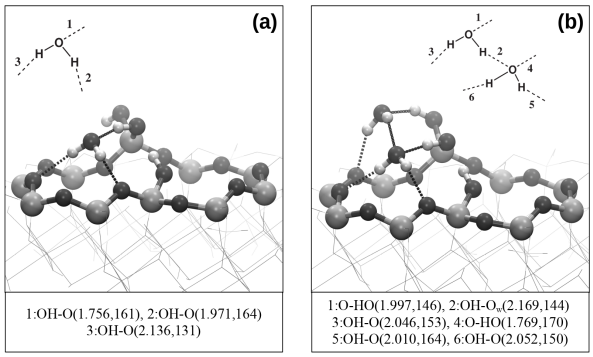

Figure 9: Optimized adsorption geometries of one (a) or two (b) WMs on the HNT(Si-OH) surface. Hydrogen bonds parameters are reported in the insets.

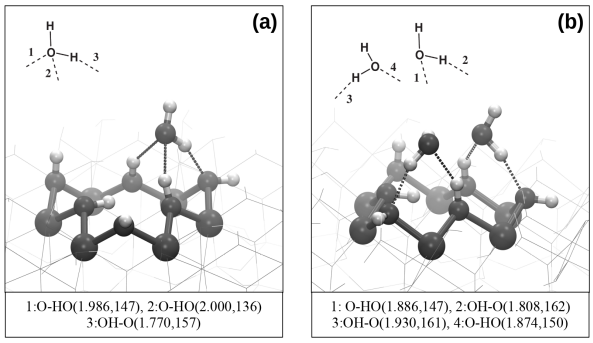

Figure 10: Optimized adsorption geometries of one (a) or two (b) WMs on the aluminic surface of HNT. Hydrogen bonds parameters are reported in the insets.

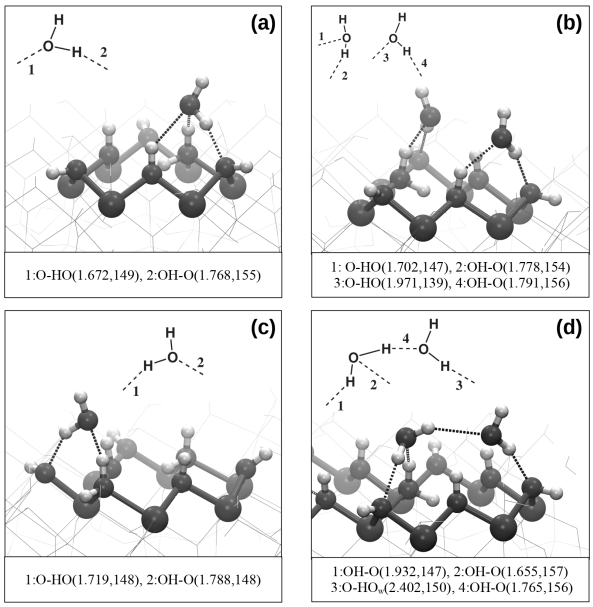

Figure 11: Optimized adsorption geometries of one (a) or two (b) WMs on the HNT(AlO-H) surface and one (c) or two (b) WMs on the HNT(AlO-H/AlO-H,p) surface. Hydrogen bonds parameters are reported in the insets.

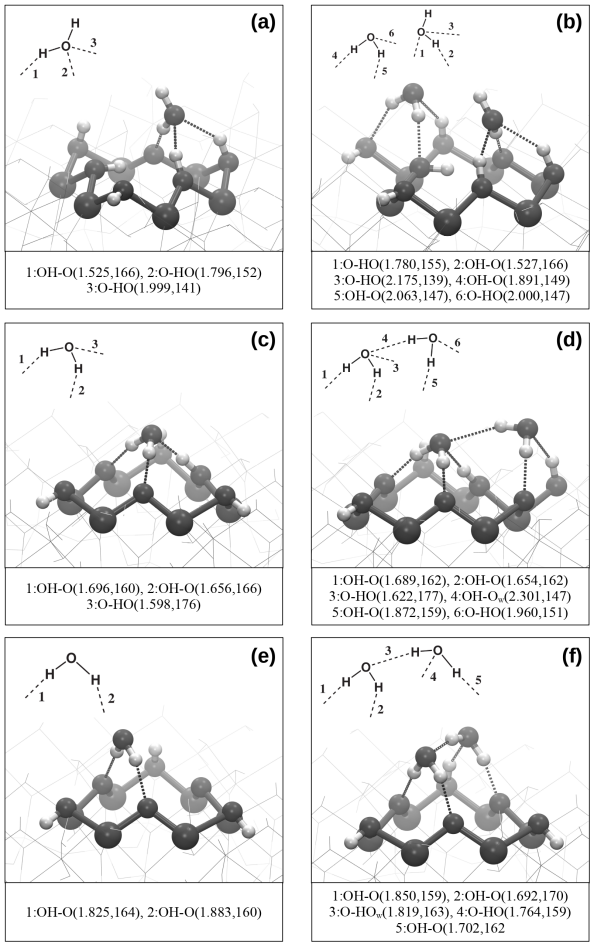

Figure 12: Optimized adsorption geometries of one (a,c,e) or two (b,d,f) WMs on the HNT(AlO^-), HNT(AlO^{2-}) and HNT(AlO^{3-}) surfaces, respectively. Hydrogen bonds parameters are reported in the insets.

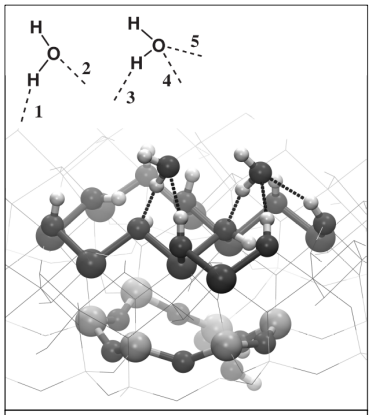

Figure 13: Adsorption geometries of two water molecules on the aluminic layer of HNT(Si-OH)Ḣydrogen bond parameters are reported in the inset.

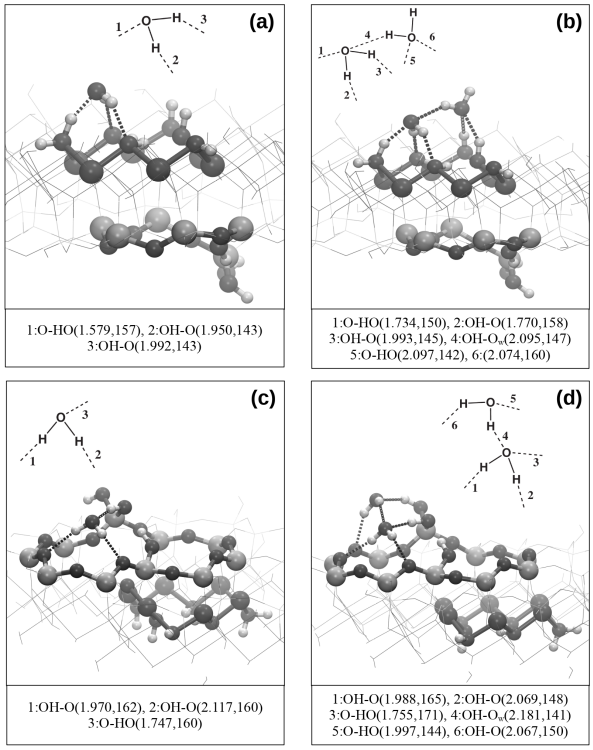

Figure 14: Optimized adsorption geometries of one (a,c) or two (b,d) WMs on aluminic and silicic layer, respectively, of the HNT(AlO-H/Si-OH) system . Hydrogen bonds parameters are reported in the insets.

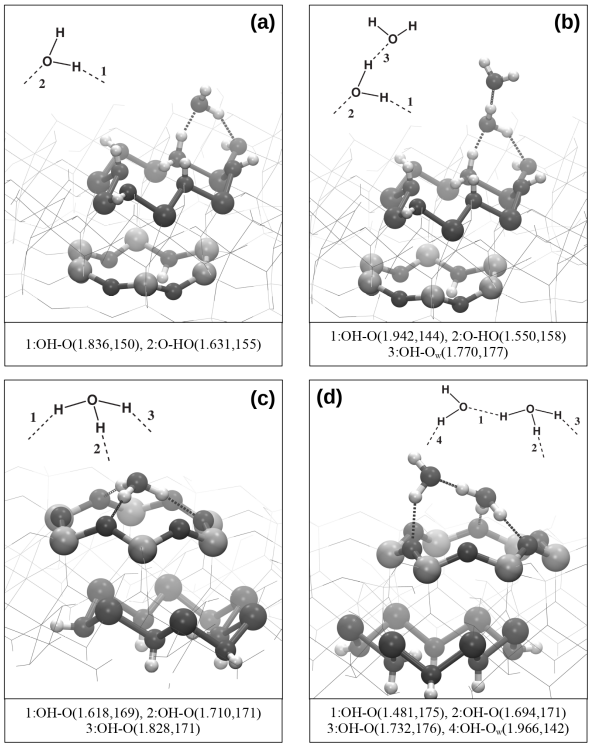

Figure 15: Optimized adsorption geometries of one (a,c) and two (b,d) WMs on the aluminic and silicic layer, respectively, of the HNT(AlO-H/SiO-H) system. Hydrogen bonds parameters are reported in the insets.

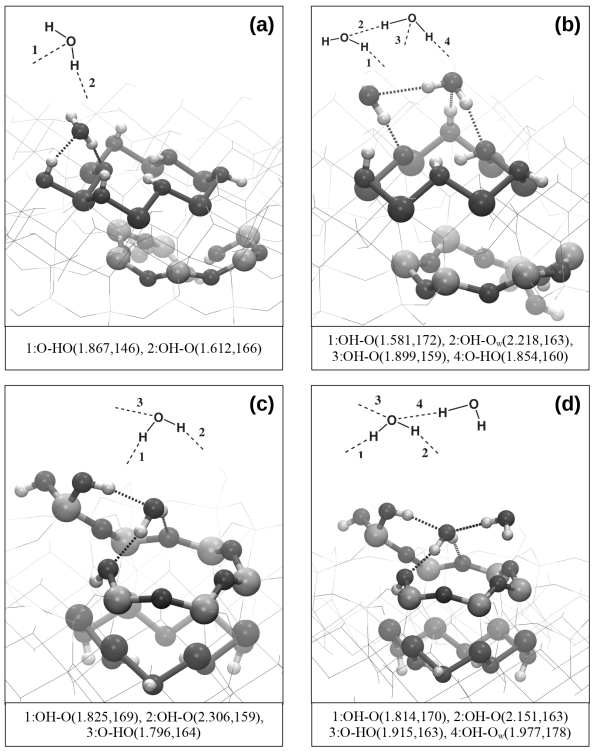

Figure 16: Optimized adsorption geometries of one (a,c) and two (b,d) WMs on the aluminic and silicic layer, respectively, of the HNT(AlO^-/Si-OH) system. Hydrogen bonds parameters are reported in the insets.

List of Tables

Table 1: The BSSE-corrected interaction energies of one or two water molecules on the halloysite surface with various superficial charge. The systems where H_3O^+ formation occurs are marked with an asterisk. It is intended that the reported interaction energy in a W_2-surface system is referred to the WM + W-surface → W_2-surface process. A notation such, for example, (Al)-AlO^-/SiO-H means that WMs adsorption occurs on the aluminic surface of the HNT(AlO^-/SiO-H) system.

	ΔE_{ads} / kJ mol^{-1}	
Surface	**W-**	**W_2-**
Al	−52.2	−36.9
Si(mode I)	−16.0	−25.7
Si (mode II)	−11.1	−35.0
AlO-H	−69.9	−54.1
SiO-H	−129.7*	−41.0
AlO-H/AlO-H,p	−66.9	−65.7
SiO-H/SiO-H,p	−78.6	−185.7*
AlO^-	−75.5	−59.2
AlO^{2-}	−110.9	−72.7
AlO^{3-}	−93.5	−114.1
Si-OH	−60.4	−35.1
(Al)-AlO^-/SiO-H	−78.1	−49.5
(Si)-AlO^-/SiO-H	−130.3*	−45.6
(Al)-AlO-H/Si-OH	−74.6	−27.6
(Si)-AlO-H/Si-OH	−60.8	−36.9
(Al)-AlO-H/SiO-H	−75.4	−46.7
(Si)-AlO-H/SiO-H	−164.6*	−59.1
(Al)-AlO^-/Si-OH	−80.5	−83.2
(Si)-AlO^-/Si-OH	−114.3*	−33.9

Table 2: Differences (with respect to unmodified HNT) on the BSSE-corrected adsorption energies of one and two water molecules on halloysite surfaces in which a charge modification is introduced on the layer opposite to the one where the adsorption occurs.

	$\Delta\Delta E_{ads}$ / kJ mol^{-1}	
Surface	**W-**	**W$_2$-**
positive charge on other side		
Si(mode I)	−9.8	+4.3
Si(mode II)	+4.4	−9.5
Al	+7.5	−0.3
negative charge on other side		
Si (mode I)	+2.1	+1.4
Si (mode II)	−5.3	+4.6
Al	−14.1	−18.0